ORIGINAL PAPER

Keegan J. Moore · Alexander F. Vakakis

Wave non-reciprocity at a nonlinear structural interface

Abstract The principle of reciprocity is a basic feature of linear structural dynamics and acoustics. This work studies the passive break of reciprocity in two linear structural waveguides coupled by an unsymmetric nonlinear interface possessing mass, linear stiffness, and clearance nonlinearities. We show that the asymmetry and nonlinearity of the connection break reciprocity even with symmetric boundary conditions, and in some cases enable one-way transmission of propagating wavepackets in a preferential direction. A quantitative measure of non-reciprocity is introduced and applied to systematically study the effect of the clearance nonlinearities for two cases: an asymmetric system with dual identical clearance nonlinearities and an asymmetric system with dual unequal clearances. In the case of the asymmetric system with dual identical clearances, we demonstrate that the effectiveness of the non-reciprocity depends on whether incident waves at the structural interface encounter the clearance nonlinearities in series or in parallel. Finally, by considering interfaces with differing clearances, we show that it is possible to realize unidirectional propagation, i.e., preferential wave transmission in one direction and prevention of wave transmission in the reverse direction. These results demonstrate the efficacy of passively controlling the flow of energy in elastic waveguides using joints with clearance nonlinearities.

1 Introduction

Acoustic reciprocity is a well-known property of linear time-invariant (LTI) waveguides, going back to the work of Helmholtz [1] and Stutt (Lord Rayleigh) [2]. More generally, in linear mechanics, the Betti–Maxwell reciprocity theorem applies, and in dynamics and acoustics reciprocity is directly related to time-reversal symmetry through the Onsager–Casimir principle of microscopic reversibility [3–5].

It is well known that reciprocity (and time-reversal symmetry) can be broken in LTI systems by introducing *odd-symmetric external biases* [6–8], *time-variant properties* [9,10], or *nonlinearities* [11–19]. In this work, wave non-reciprocity is introduced at a nonlinear interface between two elastic rods. The mass in the interface is realized by a nonlinear oscillator (NO), which is linearly or nonlinearly coupled to the ground and/or each rod. The nonlinearity is achieved by using two clearance nonlinearities: The first couples the NO to the ground, and the second couples the NO to the right rod. We consider two cases, namely a system with identical clearances or differing clearances. In both cases, the second clearance nonlinearity coupling the mass at the interface with

K. J. Moore (✉) · A. F. Vakakis
Department of Mechanical Science and Engineering, University of Illinois, Urbana, IL 61801, USA
E-mail: kmoore14@illinois.edu

A. F. Vakakis
E-mail: avakakis@illinois.edu

one of the rods breaks the symmetry and allows for extreme non-reciprocity, localization, and wave isolation. Section 2 is devoted to describing the system and developing a quantitative measure of non-reciprocity, which is employed to demonstrate the relative loss of reciprocity between the symmetric and asymmetric cases. Section 3 is divided into two subsections each describing the computational results of the aforementioned cases, demonstrating progressively increasing non-reciprocity. This work ends with a summary of the main findings and some concluding remarks.

2 Preliminary formulation and concepts

2.1 The system of nonlinearly coupled waveguides

We study the breaking of acoustic reciprocity in the system of nonlinearly coupled waveguides depicted in Fig. 1a. The system is composed of two linear, finite elastic rods with equal length and fixed-interface boundaries. Wave propagation in each of the two linear rods is governed by the classical one-dimensional (1D) wave equation. The rods are coupled to an intermediate strongly nonlinear oscillator (NO), which is coupled to the ground by a spring with clearance nonlinearity. A second clearance nonlinearity couples the NO to the left end of the right rod. The force–displacement law governing the clearance nonlinearity is depicted in Fig. 1b.

The system has been nondimensionalized such that the displacements and the clearances at the interfaces are scaled by the (common) length of the rods. We label the left rod by subscript 1 and the right rod by subscript 2. It follows that the normalized equation of motion in each of the two rods is given by,

$$u_{i,\tau\tau} + \lambda u_{i,\tau} - u_{i,\xi\xi} = P_i(\tau)\,\delta(\Delta_i), \quad i = 1, 2 \tag{1}$$

where $u_i(\tau, \xi)$ is the normalized axial deformation of rod i, τ and ξ denote the normalized temporal and spatial independent variables, respectively, and the short-hand notation is used to denote the partial derivatives, for example, $(\cdot)_{\tau\tau} \equiv \partial^2(\cdot)/\partial\tau^2$. We note at this point that a *local reference system* is used for each of the two rods, meaning that for each of the rods, we use the same notation for the normalized spatial coordinate in the range $\xi \in [0, 1]$. In (1), λ is the normalized viscoelastic damping coefficient (set to 0.1 for all cases), $P_i(\tau)$ is the normalized applied impulsive force, and $\delta(\Delta_i)$ is the Dirac's generalized function indicating the existence of the interface at the normalized position $\xi = \Delta_i$ of the left or the right rod—see the notation introduced in Fig. 1a.

Similarly, the equation of motion governing the dynamics of the intermediate NO at the interface is

$$m\ddot{y} + k_3 y - k_1 z_1 - k_2 z_2 + K_1(y - \phi(y, \varepsilon_1)) - K_2(z_2 - \phi(z_2, \varepsilon_2)) = 0, \tag{2}$$

where $y(\tau)$ is the normalized displacement of the NO, $K_i(\cdot), i = 1, 2$ are normalized nonlinear stiffness (clearance) characteristics at the interface, and

$$z_1(\tau) = u_1(1, \tau) - y(\tau),$$
$$z_2(\tau) = u_2(0, \tau) - y(\tau),$$
$$\phi(z, \varepsilon) = \begin{cases} z & z < \varepsilon, \\ \varepsilon\,\mathrm{sgn}(z) & z \geq \varepsilon. \end{cases} \tag{3}$$

The function $\phi(z, \varepsilon)$ in the last of relations (3) models the clearance nonlinearity through the sign function; the profile of the clearance nonlinearity is presented in Fig. 1b. The left and right boundaries of the left and right rods, respectively, are fixed, i.e., $u_1(0, \tau) = u_2(1, \tau) = 0$, and the interface boundary conditions are given by:

$$u_{1,\xi}(1, \tau) = -k_1 z_1,$$
$$u_{2,\xi}(0, \tau) = -k_2 z_2 - K_2(z_2 - \phi(z_2, \varepsilon_2)). \tag{4}$$

Finally, both the rods and the intermediate NO at the interface have zero initial conditions at the time of application of the external impulsive load.

To study wave non-reciprocity in this system, we will consider two different impulsive loading scenarios (LSs) while fixing the maximum impulse intensity to a constant level. First, the left rod is excited by the impulsive load $P(\tau)$ at position $\xi = \Delta_1$ (Loading Scenario I—LS I); in terms of the previous notation in (1), LS I corresponds to $P_1(\tau) = P(\tau)$ and $P_2(\tau) = 0$. Second, the right rod is excited at position $\xi = \Delta_2$
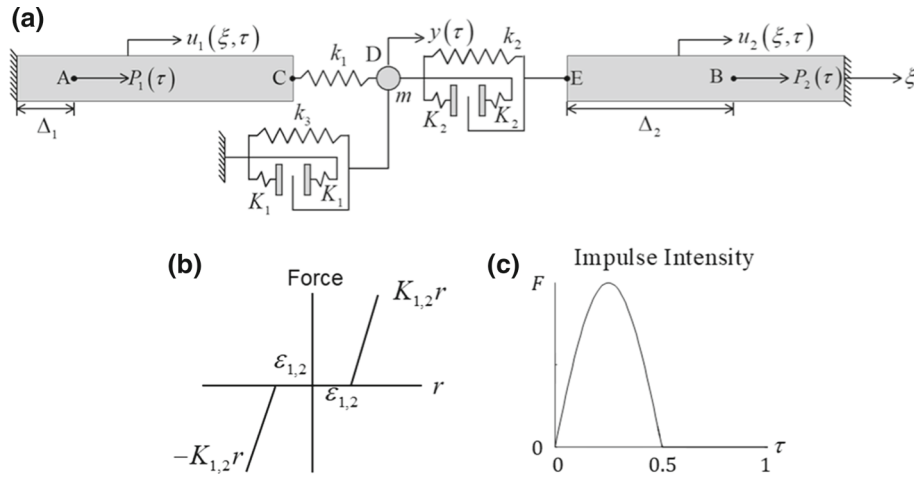
Fig. 1 System of two elastic waveguides coupled by a strongly nonlinear interface: **a** schematic of the system with the points A, B, C, D, and E corresponding to those discussed in the text and other figures, **b** the nonlinear stiffness law governing the clearance nonlinearity, and **c** the profile and intensity of the applied impulsive load

by the impulsive load $P(\tau)$ (LS II); in terms of the notation in (1), LS II corresponds to $P_1(\tau) = 0$ and $P_2(\tau) = P(\tau)$. In this work, the impulsive load

$$P(\tau) = F \sin(2\pi\tau)(\Theta(\tau) - \Theta(\tau - 0.5)) \tag{5}$$

is used, where $\Theta(\tau)$ is the Heaviside generalized function and F is the maximum impulse intensity. The profile of the applied impulsive forcing is depicted in Fig. 1c. For all cases considered in this work, we set $\lambda = 0.1$, $m = 0.05$, $k_1 = k_3 = 0.1$, $K_1 = 1000$, and $\varepsilon_1 = 0.1$, leaving the parameters k_2, K_2, ε_2 and F to vary in each case. The impulsive response of the two elastic rods was numerically modeled using finite elements with 100 elements (101 nodes) per rod.

2.2 Quantification measures of acoustic non-reciprocity

To study acoustic non-reciprocity in the system of Fig. 1, we consider N points on each rod. We evaluate the response at the position $\xi = \Delta_2$ at the right rod, $u_2(\Delta_2, \tau)$, due to an impulsive load applied at the position $\xi = \Delta_1$ at the left rod (LS I). To assess non-reciprocity in the acoustics of the system, we compare the previous responses to the response at the position $\xi = \Delta_1$ at the left rod, $u_1(\Delta_1, \tau)$, due to the same impulsive load at position $\xi = \Delta_2$ at the right rod (LS II). Clearly, for reciprocity to hold, it should hold that

$$u_1(\Delta_1, \tau) - u_2(\Delta_2, \tau) = 0, \quad \tau \geq 0, \tag{6}$$

where $\Delta_1 = mN^{-1}$ and $\Delta_2 = nN^{-1}$ for $m = 2, \ldots, N$ and $n = 1, \ldots, N - 1$. Note that $m = 1$ and $n = N$ correspond to the fixed boundaries on the left and right rods, respectively. It follows that a metric for non-reciprocity in the system of coupled waveguides can be defined by considering the integral of the difference (6) squared:

$$\theta_{m,n} = \frac{1}{T} \int_0^T (u_1(\Delta_1, \tau) - u_2(\Delta_2, \tau))^2 \, d\tau, \quad m = 2, \ldots, N, \quad n = 1, \ldots, N - 1. \tag{7}$$

This measure should result in zero for a reciprocal response and in a value greater than zero for a non-reciprocal response. Moreover, given that the previous metric is unnormalized, we may normalize it by dividing it by the product of the root-mean-square of each response, resulting in the following normalized non-reciprocity quantification measure:

$$\eta_{m,n} = \frac{\int_0^T (u_1(\Delta_1, \tau) - u_2(\Delta_2, t))^2 \, d\tau}{\sqrt{\int_0^T (u_1(\Delta_1, \tau))^2 \, d\tau} \sqrt{\int_0^T (u_2(\Delta_2, t))^2 \, d\tau}}, \quad m = 2, \ldots, N, \quad n = 1, \ldots, N - 1. \tag{8}$$

We note that this metric was first introduced in [15] for quantifying the nonlinear effects in a beam with a local stiffness nonlinearity and provides a quantitative measure of the loss of reciprocity in a normalized sense. It follows that for the underlying linear, time-invariant system, it should hold that $\eta_{m,n} = 0$, $m = 2, \ldots, N$, $n = 1, \ldots, N - 1$, but for the nonlinear system, $\eta_{m,n}$ may not be zero even if the positions of the loading are symmetric in the two rods.

3 Non-reciprocal wave transmission through the nonlinear interface

3.1 Case 1: Asymmetric interface with two identical clearances

In this section, we study the case of the asymmetric interface with two identical clearances (cf. Fig. 1). Clearly, the presence of the second clearance perturbs the overall symmetry of the system and as we show below affects significantly acoustic non-reciprocity. We set the following values for the interface parameters, $k_2 = 0.1$, $K_2 = 1000$, $F = 100$, and $\varepsilon_2 = 0.1$, such that both nonlinear elements have identical clearances and stiffnesses. The stiffness values are selected such that the components are weakly coupled and the clearance nonlinearity is strongly nonlinear and introduces a large increase in the coupling between the NO and ground, and the NO and the left boundary of the left rod. The inclusion of the second nonlinearity breaks the symmetry in the system and induces non-reciprocity in the dynamics even though symmetric boundary conditions are present at the ends of the two rods.

We start by considering the LSs I and II described in Sect. 2.1 for the specific values of the sensing and forcing locations, namely $\Delta_1 = 0.01$ and $\Delta_2 = 0.99$, representing the nodes closest to the fixed boundary in each rod. For acoustic reciprocity to hold, the response at $\Delta_2 = 0.99$ for LS I should be equivalent to the response at $\Delta_1 = 0.01$ for LS II; we present these responses as well as the difference between the two responses for impulse amplitudes of 1 and 100 in Fig. 2a, b, respectively. For an impulse amplitude of 1, we find that the displacements are identical such that the difference is zero for the entire simulation window (the actual difference is on the order of 10^{-16}, and this results from small truncation errors incurred by numerical integration). Clearly, for such a low impulse, the response is so low that the clearance nonlinearity does not engage and the system is reciprocal. For the impulse amplitude of 100, we note that the corresponding responses are not even of the same order of magnitude, such that the difference is dominated by the first response. This result warrants further discussion regarding the nonlinear mechanics governing the interactions between the waves impinging at the interface and the two clearance nonlinearities.

Considering LS I, the incident wave encounters the weak, linear coupling at the interface and is mostly reflected back into the left rod; moreover, the portion that is transmitted to the intermediate NO encounters both clearance nonlinearities simultaneously (i.e., in parallel). When the NO's displacement exceeds the clearance, the transmitted wave stops deforming the clearance nonlinearity and, instead, small-amplitude wavepackets
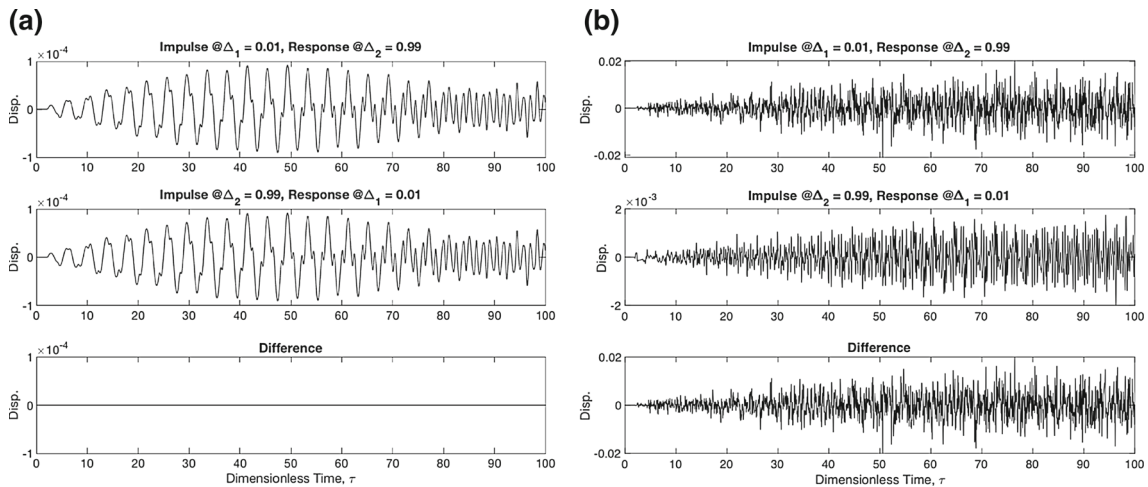

Fig. 2 Displacement of point B, $u_2(\tau, 0.99)$, for an impulse applied at $\Delta_1 = 0.01$; the displacement of point A, $u_1(\tau, 0.01)$, for an impulse applied at $\Delta_2 = 0.99$; and the difference of the two displacements: plotted for an impulse amplitude of **a** 1 and **b** 100
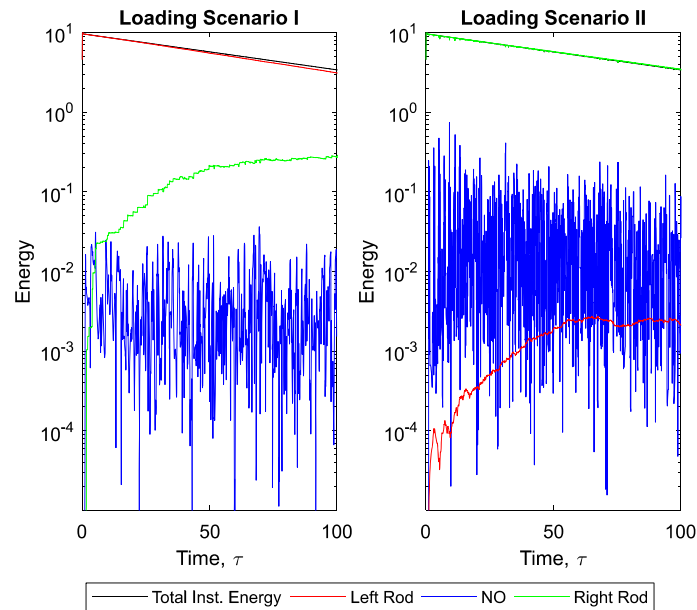
Fig. 3 Instantaneous total energy stored in each rod and the NO for each of the two loading scenarios (LSs)

are transferred into the right rod. This occurs because the compliance of the rod is much greater than that of the engaged clearance nonlinearity, and the system achieves a lower energy state by deforming the rod instead of the clearance nonlinearity. The resulting outcome of this interaction is small energy transfers to the right rod such that the energy in the left and right rod gradually decreases and increases, respectively, as time increases. To verify this, in Fig. 3a we plot the sum of the kinetic and potential energies of the two rods and the NO for the LS I. The energy in the coupling springs and the second nonlinearity were neglected in the computation of these energy plots. Figure 3a confirms that most of the energy is confined in the left rod (due to the intense reflections at the interface) and that energy is transferred to the right rod in small amounts.

A different energy transfer scenario is realized for LS II. In that case, the incident wave from the right rod encounters a weak, linear coupling and the second clearance nonlinearity at the boundary and, just as in LS I, much of the wave is reflected into the right rod (where it is originally generated). However, in contrast to LS I, the transmitted wave now encounters the clearance nonlinearities separately (in series). As such, the boundary of the right rod initially deforms freely (due to the large compliance of the unengaged clearance nonlinearity and the coupling spring), until its displacement equals the clearance ε_2. At this point, the compliance of the clearance nonlinearity drops below that of the NO, and the transmitted wave propagates into the NO. Unlike LS I (where the right boundary of the left rod maintains large displacements), the second clearance nonlinearity prevents the boundary from achieving large displacements. When the transmitted wave reaches the NO, it encounters the first clearance nonlinearity and the linear coupling springs simultaneously (in parallel). The transmitted wave displaces the NO until the first clearance nonlinearity is engaged, at which point the transmitted wave reflects off the ground and propagates back into the right rod. As the wave is displacing the NO, some energy transfers into the left rod; however, the energy transfer is terminated each time the wave is reflected off the ground. Consequently, much less energy is transferred to the left rod in LS II than is transferred to the right rod in LS I, so strong acoustic non-reciprocity is realized. Figure 3b depicts the energies in the rods and the NO (with the energies at the clearances omitted from the computation) and confirms that most of the energy remains in the right rod (due to the large reflections at the interface) and that very little energy is transferred into the left rod. It follows that the asymmetrical nonlinear interface differentiates between left-to-right and right-to-left wave transmission and leads to nonlinear non-reciprocity in a predictable way.

In Fig. 4a, b, we present the displacement of points C, D, E and the relative displacement between the NO and the unexcited rod for LSs I and II, respectively. The displacements of points C and E for LS II are presented on the same scales as the displacements of E and C for LS I, respectively, which allows for a direct comparison of the wave transmission. We find that the displacement of point E in LS II is approximately 10% of that observed at point C in LS I, which reflects the fact that point E is restricted by the second clearance nonlinearity, whereas point C is weakly restricted by the linear coupling. A similar result is found by comparing the displacement
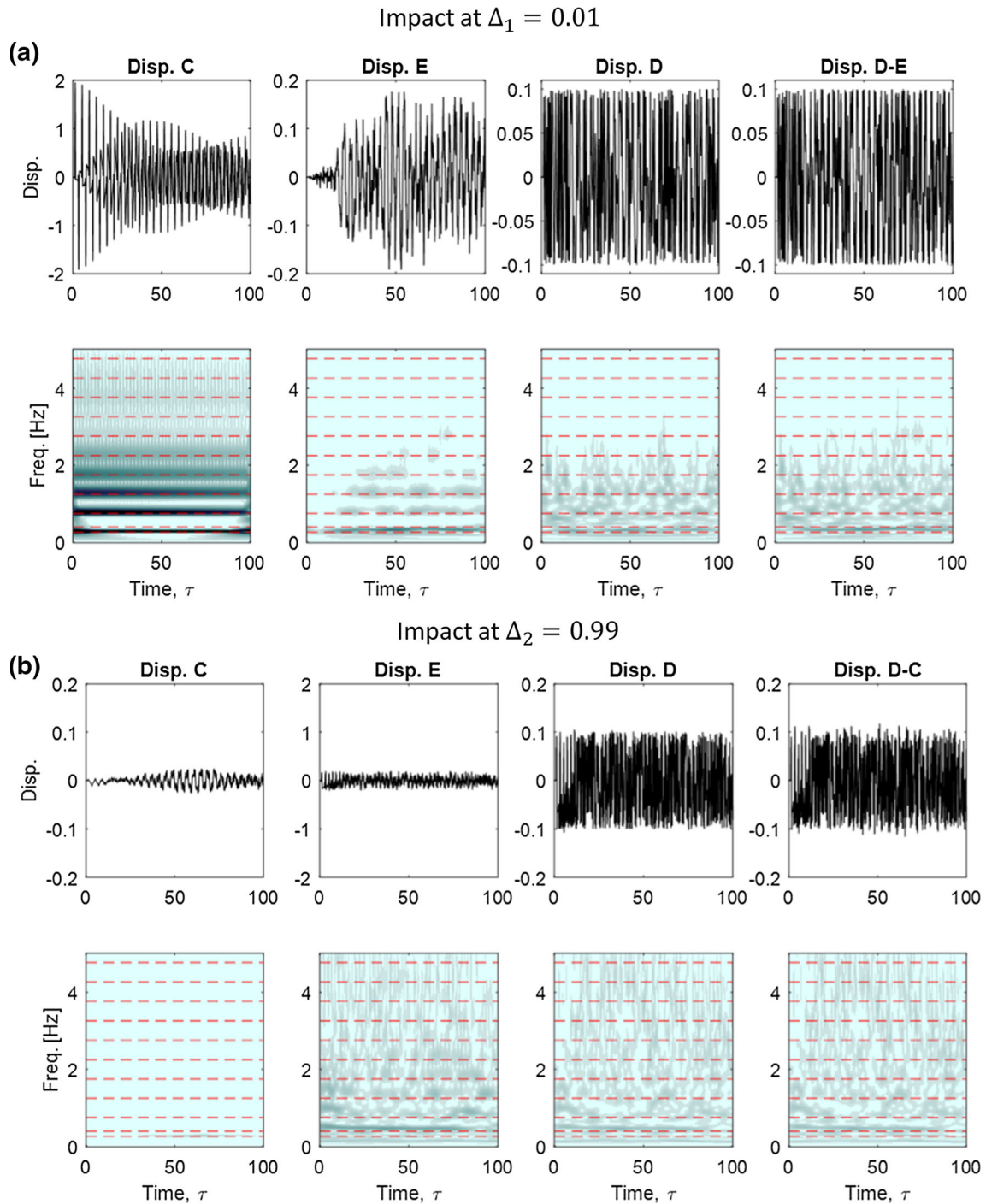
Fig. 4 Displacement and the corresponding WT spectra at points D, C, and E and the relative displacement between the NO and the unexcited rod for **a** LS I and **b** LS II

of point D in LS I with that of point C in LS II, which reflects the difference in energy propagation to the unexcited rod in each LS. The WT spectrum of the displacement of point C for LS I reveals that the response is governed by the modes of the underlying linear system, which are overlaid onto the WT spectra as dashed lines. In contrast, the harmonics governing the displacement of point E in LS II are shifted above the linear natural frequencies and reflect the increased stiffness contributed by the clearance nonlinearity. Note that the amplitudes of the WT spectra are all plotted on the same scale with the lightest shade representing 0 and the
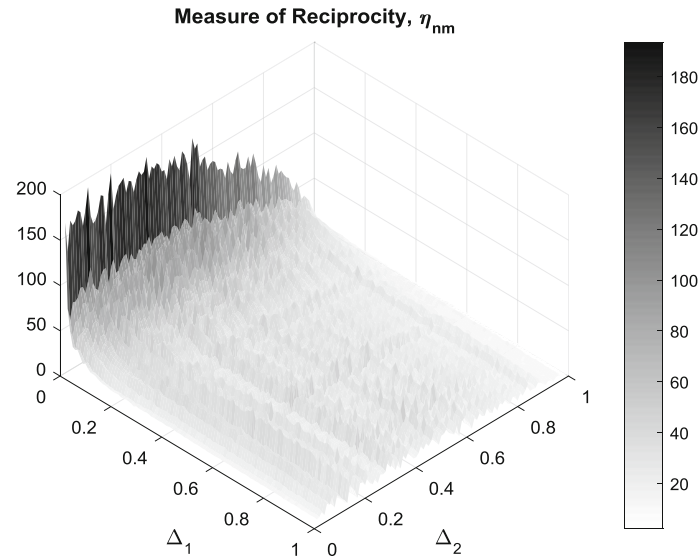
Fig. 5 Measure of non-reciprocity, $\eta_{m;n}$, plotted a three-dimensional surface with color plot overlaid

darkest shade representing 0.5 or higher. Moreover, the scattering effect of the clearance nonlinearity is clearly observed in the WT spectrum, which is absent in the WT spectrum of the displacement of point E in LS I. This reflects the fact that more energy is stored in the second clearance nonlinearity during LS II than in LS I. On this scale, only the fundamental harmonic is visible in the WT spectrum of the displacement of point C in LS II, whereas several harmonics are visible for that of point E in LS I, which results from the difference in energy that propagates into the unexcited rod in each LS. Looking at the WT spectra of point D for both LSs, we find that both capture the scattering effect of the clearance nonlinearity; however, the scattering is more pronounced and reaches higher frequencies for LS II, which confirms that more energy is stored in the clearance nonlinearities in LS II than in LS I.

Lastly, we consider the measure of non-reciprocity described in Sect. 2.2 for this asymmetric case. In Fig. 5, we plot this measure for LSs I and II applied to each node of the two rods, by varying the parameters Δ_1 and Δ_2 of the forcing and sensing positions. In that way, we gain a complete understanding of the nonlinear non-reciprocity in the system of Fig. 1 for the specific level of the applied impulsive excitation. We emphasize at this point that since the interface is nonlinear, it is expected that the non-reciprocity results reported here will change as the energy level of the wave interaction at the interface changes (this, however, is not considered in this work). Considering the plots of Fig. 5, the regions depicted in white correspond to regions where the wave non-reciprocity is small; however, these regions are still non-reciprocal, with the minimum value being $\eta_{100;99} = 2.211$ for $\Delta_1 = 1$ and $\Delta_2 = 0.99$. We note that the minimum measure of reciprocity for this systems is over five times larger than that for the symmetric system studied in Sect. 3.1. We note that Fig. 5 contains bands of strong non-reciprocity; however, the bands are much harder to distinguish, no large white regions are present, and no apparent symmetries are present. In fact, a clear preference is seen in the plot with the measure of non-reciprocity rapidly increasing as $\Delta_1 \rightarrow 0.01$, with the maximum occurring at $\Delta_1 = 0.01$ and $\Delta_2 = 0$ with a maximum value of $\eta_{2;1} = 193.52$, which is nearly six times the maximum of the previous system. For these values of $\Delta_{1,2}$, the excitation is furthest from and closest to the interface in LSs I and II, respectively. This results in the energy transferred to the interface being minimized and maximized in LSs I and II, respectively. Additionally, we present the non-reciprocity parameter for varying impulse amplitude applied to five locations on each rod in Fig. 6. Specifically, we simulate the response of the system to an impulse applied to each of the ten locations (five per rod) for 212 amplitudes spaced logarithmically from 10^{-2} to 10^8. The plots reveal that the dynamics can be partitioned into three regimes: two linear, reciprocal regimes at low and high forcing and a nonlinear, non-reciprocal regime that "bridges" the two linear regimes.

3.2 Case 2: Asymmetric interface with two different clearances

In this second section, we study the case of the asymmetric interface with two different clearances, and, to this end, we consider the system parameters $k_2 = 10^{-6}$, $K_2 = 1000$, $F = 11$, and $\varepsilon_2 = 0.2$. The decrease
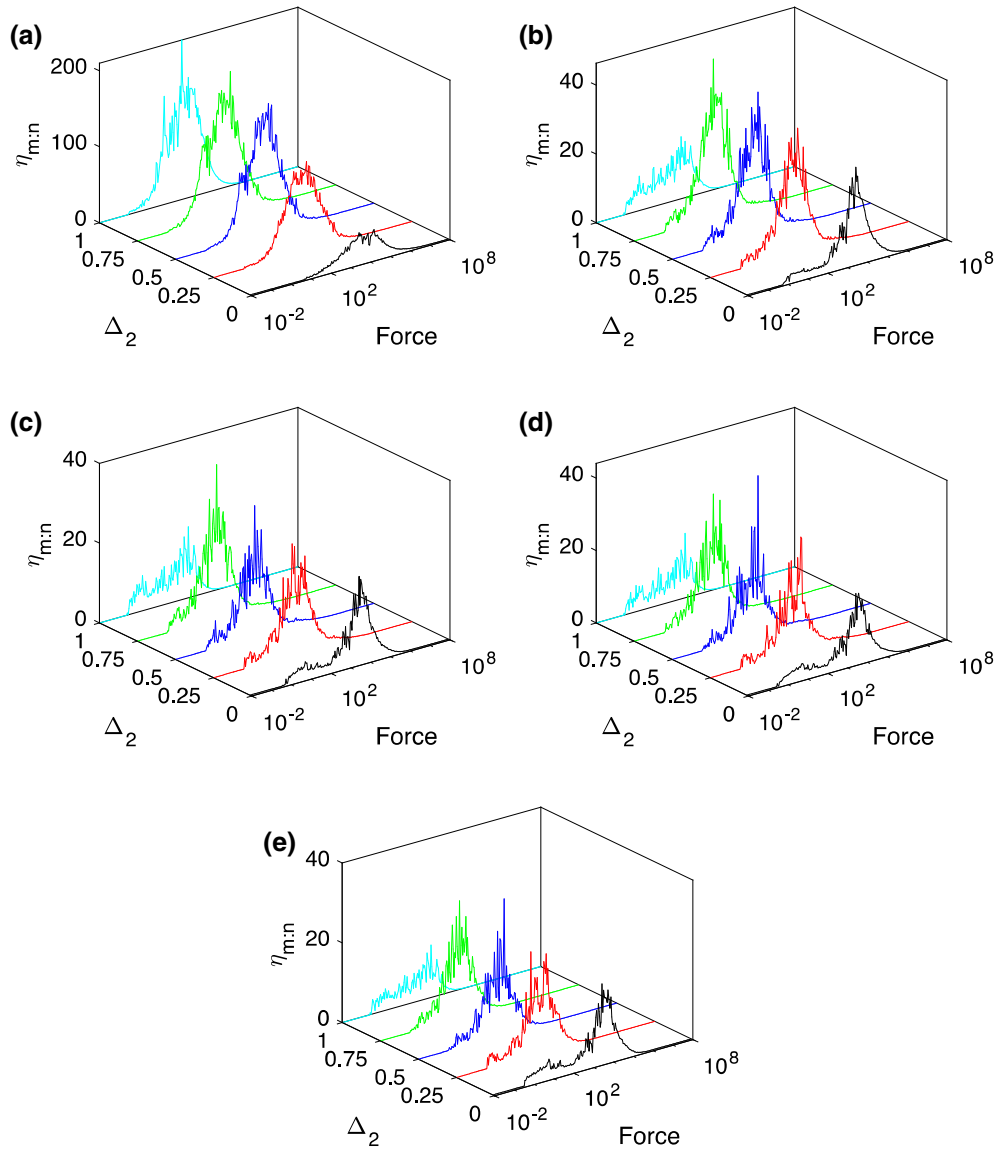
Fig. 6 Measure of non-reciprocity, $\eta_{m;n}$, computed for varying impulsive force and Δ_2 for **a** $\Delta_1 = 0.01$, **b** $\Delta_1 = 0.25$, **c** $\Delta_1 = 0.5$, **d** $\Delta_1 = 0.75$, **e** $\Delta_1 = 1$

and increase in k_2 and ε_2, respectively, were chosen to increase the non-reciprocity significantly compared to the previous cases, so much that one only needs weak forcing to achieve large-wave non-reciprocity at the interface. As in the previous case, we present the displacement response for both LSs I and II described in Sect. 2.1, and we start by considering the specific case $\Delta_1 = 0.01$ and $\Delta_2 = 0.99$. The results of wave transmission in the system of rods and at the interface are presented in Fig. 7a, b for impulse amplitudes of 1 and 10, respectively. For an impulse amplitude of 1, we find that the displacements are identical such that the difference is zero for the entire simulation window (the actual difference is on the order of 10^{-21}, and this results from small truncation errors incurred by numerical integration). Clearly, for such a low impulse, the response is so low that the clearance nonlinearity does not engage and the system is reciprocal. For the impulse amplitude of 100, we note that in contrast to the previous asymmetric case (where the displacement at $\Delta_1 = 0.01$ for LS II was an order of magnitude lower than its counterpart for LS I), the displacement at $\Delta_2 = 0.99$ for LS I has an amplitude five orders of magnitude less than its counterpart for LS II, so strong acoustic non-reciprocity is realized.
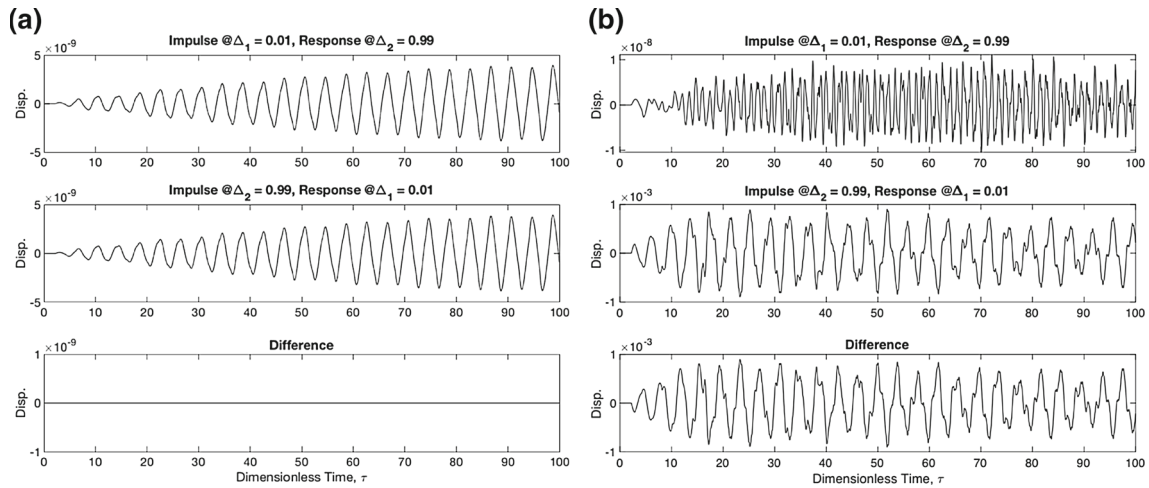
Fig. 7 Displacement of point B, $u_2(\tau, 0.99)$, for an impulse applied at $\Delta_1 = 0.01$; the displacement of point A, $u_1(\tau, 0.01)$, for an impulse applied at $\Delta_2 = 0.99$; and the difference of the two displacements: plotted for an impulse amplitude of **a** 1 and **b** 11
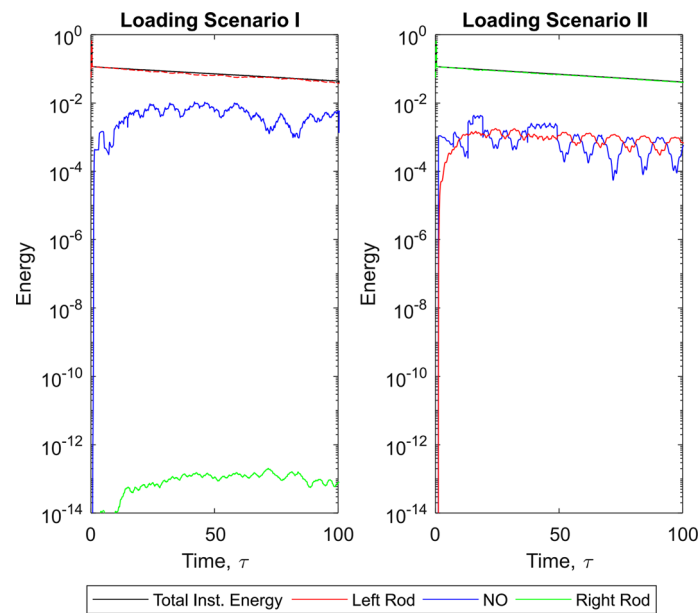

Fig. 8 Instantaneous total energy stored in each rod and the NO for each LS

Indeed, for LS I the incident wave first encounters the weak, linear coupling at the interface, so it is mostly reflected back into the left rod and, like in the case of the previous section, the portion that is transmitted to the NO encounters both clearance nonlinearities simultaneously (in parallel). When the NO's displacement equals ε_1, the transmitted wave stops deforming the clearance nonlinearity. However, unlike in the previous case, the transmitted wave cannot propagate into the right rod because the displacement of the NO is not large enough to engage the second clearance nonlinearity. Instead, the wave crosses the first clearance nonlinearity, reflects off the ground, and propagates back into the left rod. The result of this wave interaction is that almost no energy is transferred into the right rod and the interface acts as a wave arrestor. That is, due to the interface, when the left rod is excited, the system primarily behaves as if the right rod is entirely absent. To verify this, in Fig. 8a, we plot the summation of the kinetic and potential energies of each rod and the NO for LS I. As previously, the energy in the coupling springs and the second nonlinearity were neglected in the computation of the depicted energies. Figure 8a confirms that virtually no energy is transferred into the right rod, with the energy in the right rod being 12 orders of magnitude lower than that for the left rod.
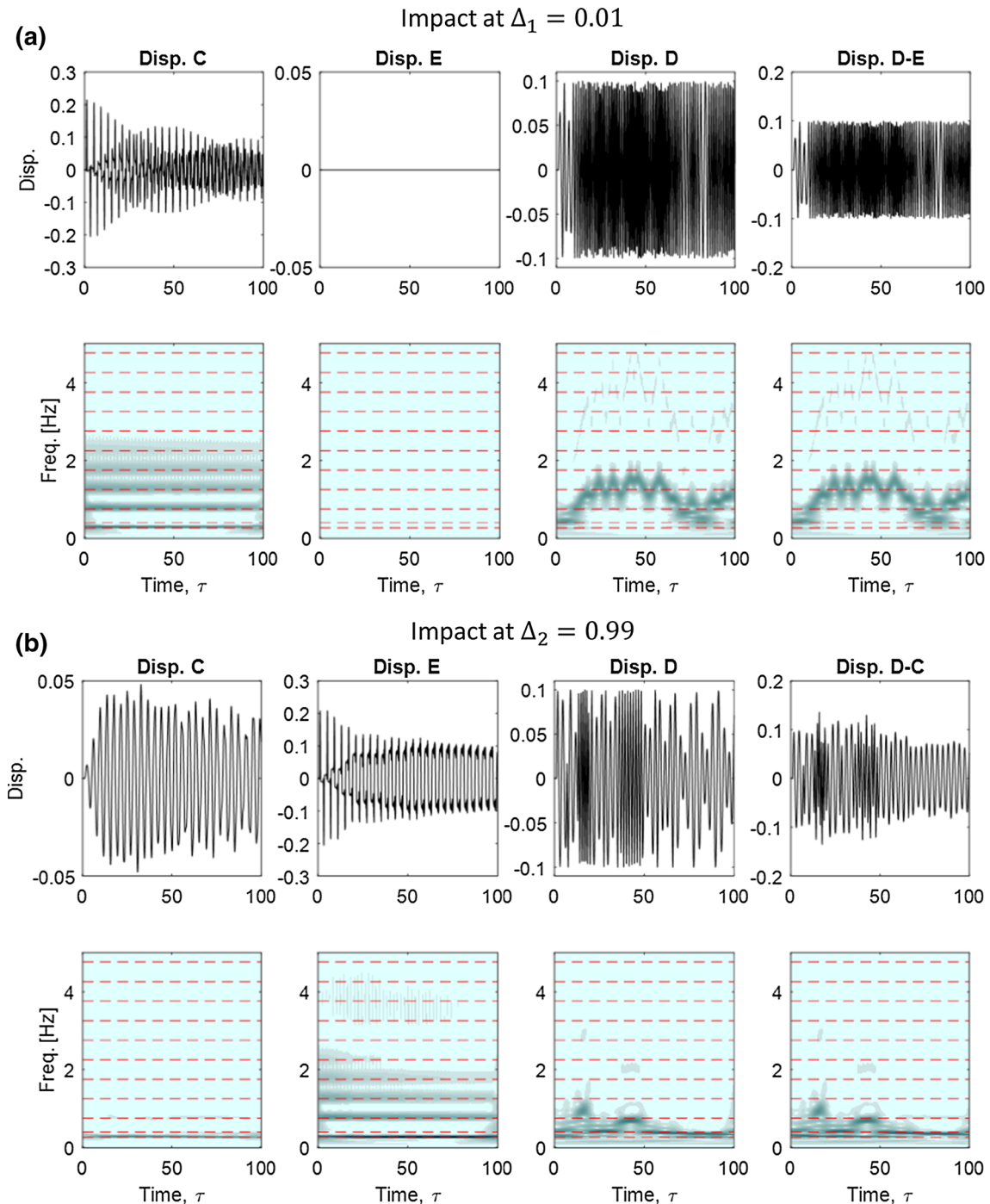
Fig. 9 Displacement and corresponding WT spectra at points D, C, and E and the relative displacement between the NO and the unexcited rod for **a** LS I and **b** LS II

The interactions and nonlinear mechanics governing the system's response for LS II are virtually the same as those described for LS II in the previous section. The main difference is that the increased clearance allows for the left end of the right rod to attain a larger amplitude of oscillation in this case. In previous case, the energy transferred to the left rod in LS II was much less than the energy transferred to the right rod in LS I. However, for this case, the opposite occurs and much more energy is transferred to the left rod for LS II than
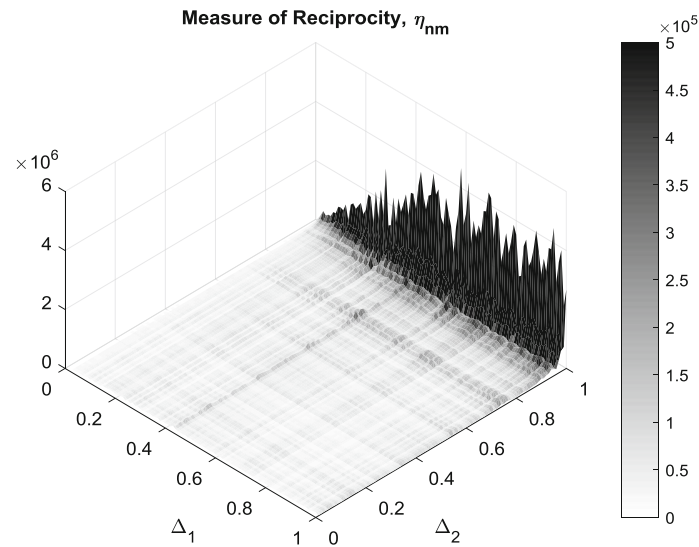
Fig. 10 Measure of non-reciprocity, $\eta_{m;n}$, plotted as a three-dimensional surface with color plot overlaid

is transferred to the right rod for LS I. Figure 8b presents the energies in the rods and the NO and confirms that significantly more energy transfers into the right rod than to the left rod in the previous case.

In Figs. 8b and 9a, we present the displacement at points C, D, E as well as the relative displacement between the NO and the unexcited rod for LSs I and II, respectively. The displacements at points C and E for LS II are presented on the same scales as the displacements of E and C for LS I, respectively, which allows for a direct comparison. We find that for LS I the displacement of point E is virtually zero, and so is significantly smaller than that observed at point C for LS II. This reflects the fact that, as discussed previously, nearly no energy is transferred into the right rod for LS I. The displacement of point E in LS II is comparable to that of point C in LS I in terms of magnitude, but due to the second clearance nonlinearity, their profiles (and frequency content) do not match. Just as in the previous cases, the WT spectrum of the displacement at point C for LS I reveals that the response is governed by the modes of the underlying linear system, which are overlaid onto the WT spectra as dashed lines.

In contrast to the previous cases, we note that for LS II the harmonics governing the displacement of point E correspond to the modes of the underlying linear system, and this results from the decreased amplitude of the impulse applied to system. Note that amplitudes of the WT spectra are all plotted on the same scale with the lightest shade representing 0 and the darkest shade representing 0.25 or higher. The scattering effect of the clearance nonlinearity that was present in the previous asymmetric case is not present in the WT spectrum and reflects the reduced amount of energy in the system. On this scale, no harmonics are visible in the WT spectrum of the displacement of point E for LS I, whereas the fundamental harmonic is visible in the WT spectrum of the displacement of point C for LS II. Looking at the WT spectrum of point D for LS I, we find that the response is governed by a single harmonic; however, that harmonic exhibits dynamic instability such that its frequency fluctuates. In contrast, the WT spectrum of point D for LS II shows multiple harmonics as well as effects from the scattering of energy to higher frequencies. These results highlight the role of the clearance nonlinearities at the interface as frequency scatters; clearly, by examining the frequency contents at the responses at the boundaries of the interface, we deduce the drastic effect that the strongly nonlinear and non-smooth interface has on the transmitted and reflected waves, resulting in higher-frequency energy scattering of the impeding waves. This frequency scattering has immediate effects on the transmission characteristics of the interface since as wave energy is scattered to higher frequencies, the amplitudes of the waves reduces significantly and their frequency content is significantly altered.

Lastly, we consider the measure of non-reciprocity described in Sect. 2.2 and plot it for both LSs I and II with an impulse amplitude of $F = 11$ applied to each node of the rods; the results are presented in Fig. 5. The regions depicted in white correspond to regions where the non-reciprocity is small; however, these regions are still strongly non-reciprocal, with the minimum value being $\eta_{1;3} = 3533.9$ for $\Delta_1 = 0.01$ and $\Delta_2 = 0.02$. We note that the minimum measure of reciprocity for this systems is three orders of magnitude larger than that for the system studied in Sect. 3.1, even though the impulse amplitude is significantly less. To improve
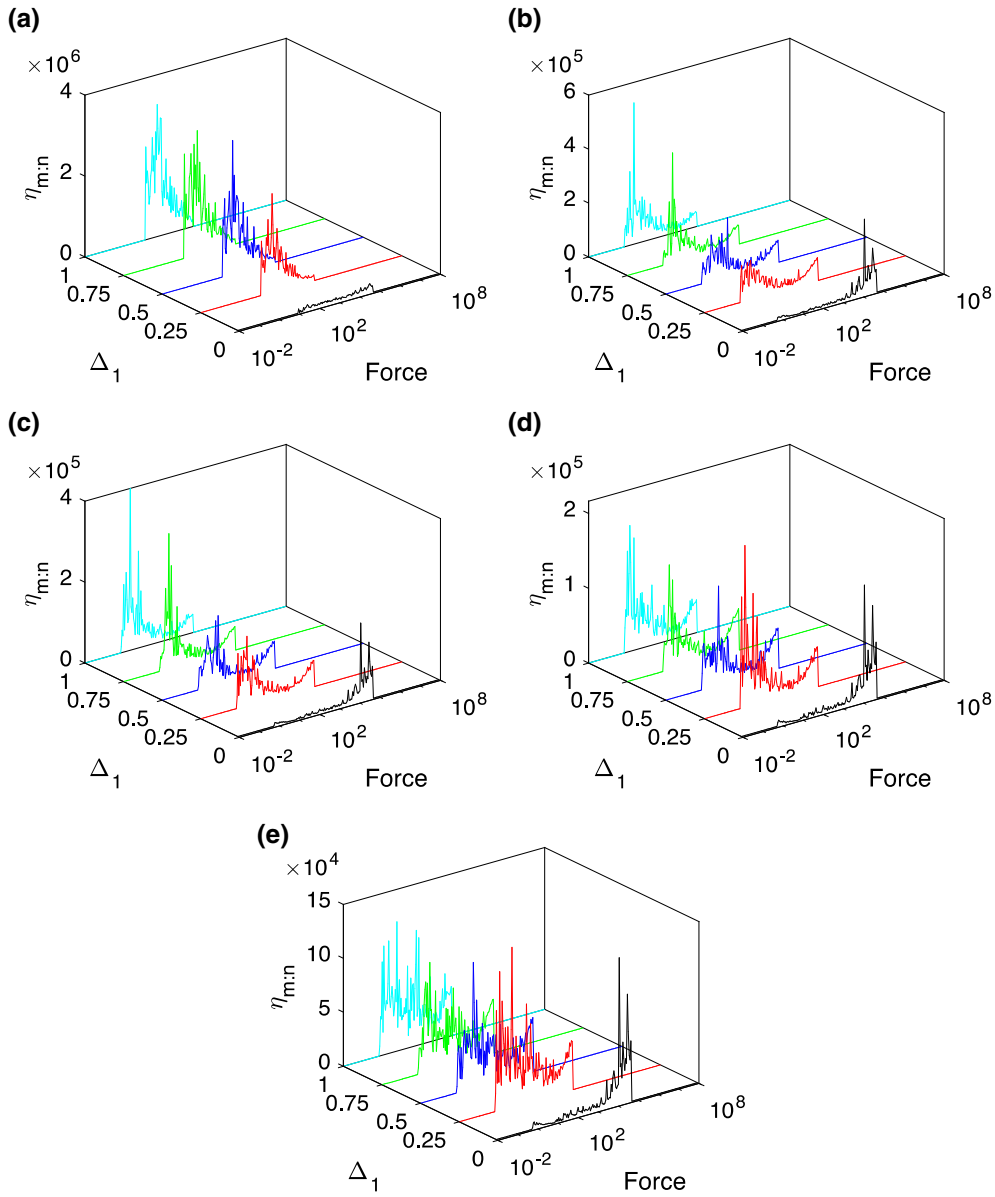
(a)

(b)

(c)

(d)

(e)

Fig. 11 Measure of non-reciprocity, $\eta_{m;n}$, computed for varying impulsive force and Δ_1 for **a** $\Delta_2 = 0.99$, **b** $\Delta_2 = 0.75$, **c** $\Delta_2 = 0.5$, **d** $\Delta_2 = 0.25$, **e** $\Delta_2 = 0$

the visibility of the plots, the maximum value of the color scale is reduced by an order of magnitude below the maximum non-reciprocity measure. Like in the previous case, Fig. 10 contains bands of strong non-reciprocity, but neither large white regions nor apparent symmetries are present in the plots. A clear preference is visible in the plots with the measure of non-reciprocity drastically increasing as $\Delta_2 \rightarrow 1$, with the maximum occurring at $\Delta_1 = 0.58$ and $\Delta_2 = 0.99$ with a maximum value of $\eta_{1;2} = 4.675 \times 10^6$, which is three orders of magnitude larger than the previous asymmetric case.

Additionally, we present the non-reciprocity parameter for varying impulse amplitude applied to five locations on each rod in Fig. 11. Specifically, we simulate the response of the system to an impulse applied to each of the ten locations (five per rod) for 212 amplitudes spaced logarithmically from 10^{-1} to 10^8. The plots reveal that the dynamics can be partitioned into three regimes: two linear, reciprocal regimes at low and high forcing and a nonlinear, non-reciprocal regime that "bridges" the two linear regimes. The jumps in the non-reciprocity measure result from the activation of the second clearance. Specifically, the first jump that occurs around a forcing of 5×10^{-1} results from the second clearance nonlinearity being engaged in LS II

but not in LS I. The second clearance nonlinearity remains engaged in LS II and not in LS I up until the jump down (around a forcing of 5×10^4), at which point the second clearance nonlinearity is engaged in both LS I and LS II. Note that even after the jump down, the non-reciprocity measure continues to be nonzero, but is significantly reduced compared to the values prior to the jump down. After the jump down, the non-reciprocity smoothly decreases as the input force amplitude increases until it converges to zero, indicating that the system exhibits a linear response.

4 Concluding remarks

We studied the response of two linear, elastic rods coupled by a nonlinear interface possessing both stiffness and mass. The mass in the interface was realized by a single nonlinear oscillator (NO), which was linearly coupled to the ground and each rod. The nonlinearity was achieved using two clearances, one of which was used to ground the NO and the other to couple the NO with the right rod.

In the first case, we considered an asymmetric interface with the clearance nonlinearities having identical clearances and stiffnesses. In this case, we found that the mechanisms governing the propagation of energy in the system depended on which rod was excited. The differences were attributed to whether the clearances were encountered in series or in parallel by the wave impeding to the interface. In the second case, we studied the asymmetric interface with different clearances, with reduced linear coupling between the NO and the right rod, and with reduced impulse intensity. We found that the interface in this case served to isolate the right rod from the left, such that if the left rod was excited, the system responded as if the right rod was disconnected. However, when the right rod was excited, the propagating wave engaged directly the left rod and the system did not respond as if either rod were disconnected. This led to strong acoustic non-reciprocity in wave transmission.

In all cases, we computed a measure of non-reciprocity (defined in Sect. 2.2) and found that the non-reciprocity significantly increases from cases 1 to 2, with extreme non-reciprocity occurring in case 3. The measure of non-reciprocity provides the option of optimizing the impulse locations, such that the effects of the nonlinearity and the loss of reciprocity are maximized. If the value of measurement points is increased, a finer set of data can be obtained resulting in a more accurate estimation of the optimal impulse location. The findings of this work show that strongly nonlinear, non-smooth interfaces can be designed for preferential wave transmission in networks of elastic systems, and this can be achieved by inducing passive nonlinear non-reciprocity through the non-smooth asymmetrical stiffness nonlinearities in the interfaces.

References

1. Helmholtz, H.V.: Theorie der Luftschwingungen in Röhren mit offenen Enden. Angew. Math. **57**, 1–72 (1860)
2. Strutt, J.W.: Some general theorems relating to vibrations. Proc. Lond. Math. Soc. **1**, 357–368 (1871)
3. Onsager, L.: Reciprocal relations in irreversible processes—I. Phys. Rev. **37**, 405–426 (1931)
4. Onsager, L.: Reciprocal relations in irreversible processes—II. Phys. Rev. **38**, 2265–2279 (1931)
5. Casimir, H.B.G.: On Onsager's principle of microscopic reversibility. Rev. Mod. Phys. **17**, 343–350 (1945). https://doi.org/10.1103/RevModPhys.17.343
6. Cummer, S.A.: Selecting the direction of sound transmission. Science **343**, 495–496 (2014). https://doi.org/10.1126/science.1249616
7. Fleury, R., Sounas, D.L., Sieck, C.F., Haberman, M.R., Alù, A.: Sound isolation and giant linear nonreciprocity in a compact acoustic circulator. Science **343**, 516–519 (2014). https://doi.org/10.1126/science.1246957
8. Tsakmakidis, K.L., Shen, L., Schulz, S.A., Zheng, X., Upham, J., Deng, X., Altug, H., Vakakis, A.F., Boyd, R.W.: Breaking Lorentz reciprocity to overcome the time-bandwidth limit in physics and engineering. Science **356**, 1260–1264 (2017). https://doi.org/10.1126/science.aam6662
9. Popa, B.-I., Cummer, S.A.: Non-reciprocal and highly nonlinear active acoustic metamaterials. Nat. Commun. **5**, 3398 (2014). https://doi.org/10.1038/ncomms4398
10. Fleury, R., Sounas, D.L., Alù, A.: Subwavelength ultrasonic circulator based on spatiotemporal modulation. Phys. Rev. B. **91**, 174306 (2015). https://doi.org/10.1103/PhysRevB.91.174306
11. Liang, B., Guo, X.S., Tu, J., Zhang, D., Cheng, J.C.: An acoustic rectifier. Nat. Mater. **9**, 989–992 (2010). https://doi.org/10.1038/nmat2881

12. Maznev, A.A., Every, A.G., Wright, O.B.: Reciprocity in reflection and transmission: What is a 'phonon diode'? Wave Motion **50**, 776–784 (2013). https://doi.org/10.1016/j.wavemoti.2013.02.006
13. Maldovan, M.: Sound and heat revolutions in phononics. Nature **503**, 209–217 (2013). https://doi.org/10.1038/nature12608
14. Zhang, J., Peng, B., Özdemir, Ş.K., Liu, Y., Jing, H., Lü, X., Liu, Y., Yang, L., Nori, F.: Giant nonlinearity via breaking parity-time symmetry: a route to low-threshold phonon diodes. Phys. Rev. B. **92**, 115407 (2015). https://doi.org/10.1103/PhysRevB.92.115407
15. Zhang, Z., Koroleva, I., Manevitch, L.I., Bergman, L.A., Vakakis, A.F.: Non-reciprocal acoustics and dynamics in the in-plane oscillations of a geometrically nonlinear lattice. Phys. Rev. E. **94**, 032214 (2016). https://doi.org/10.1103/PhysRevE.94.032214
16. Coulais, C., Sounas, D., Alù, A.: Static non-reciprocity in mechanical metamaterials. Nature **542**, 461–464 (2017). https://doi.org/10.1038/nature21044
17. Darabi, A., Leamy, M.J.: Clearance-type nonlinear energy sinks for enhancing performance in electroacoustic wave energy harvesting. Nonlinear Dyn. **87**, 2127–2146 (2017)
18. Moore, K.J., Bunyan, J., Tawfick, S., Gendelman, O.V., Shuangbao, L., Leamy, M.J., Vakakis, A.F.: Non-reciprocity in the dynamics of coupled oscillators with nonlinearity, asymmetry and scale hierarchy. Phys. Rev. E. **97**, 012219 (2018)
19. Bunyan, J., Moore, K.J., Mojahed, A., Fronk, M.D., Tawfick, S., Leamy, M., Vakakis, A.F.: Acoustic non-reciprocity in a lattice incorporating nonlinearity, asymmetry and internal scale hierarchy:experimental study. Phys. Rev. E. **97**(5), 052211 (2018). https://doi.org/10.1103/PhysRevE.97.052211